PROCEEDINGS OF SPIE

SPIEDigitalLibrary.org/conference-proceedings-of-spie

Gain dynamics in a highly ytterbium-doped potassium double tungstate thin-film amplifier

Yean-Sheng Yong, Shanmugam Aravazhi, Sergio A. Vázquez-Córdova, Jennifer L. Herek, Sonia M. García-Blanco, et al.

Yean-Sheng Yong, Shanmugam Aravazhi, Sergio A. Vázquez-Córdova, Jennifer L. Herek, Sonia M. García-Blanco, Markus Pollnau, "Gain dynamics in a highly ytterbium-doped potassium double tungstate thin-film amplifier," Proc. SPIE 10896, Solid State Lasers XXVIII: Technology and Devices, 108961G (7 March 2019); doi: 10.1117/12.2514806

SPIE.

Event: SPIE LASE, 2019, San Francisco, California, United States

Gain dynamics in a highly ytterbium-doped potassium double tungstate thin-film amplifier

Yean-Sheng Yong,[1] Shanmugam Aravazhi,[2] Sergio A. Vázquez-Córdova,[1] Jennifer L. Herek,[1] Sonia M. García-Blanco,[1] and Markus Pollnau[2,3]
[1]Optical Sciences Group, MESA+ Institute for Nanotechnology, University of Twente, P.O. Box 217, 7500 AE Enschede, The Netherlands
[2]Integrated Optical Microsystems Group, MESA+ Institute for Nanotechnology, University of Twente, P.O. Box 217, 7500 AE Enschede, The Netherlands
[3]Advanced Technology Institute, Department of Electrical and Electronic Engineering, University of Surrey, Guildford GU2 7XH, United Kingdom

ABSTRACT

Active media with high rare-earth concentrations are essential for small-footprint waveguide amplifiers. When operating at high population inversion, such devices are often affected by undesired energy-transfer processes and thermal effects. In this work, we study a 32-µm-thick epitaxial layer of potassium gadolinium ytterbium double tungstate with a high Yb content of 57at.%, representing an Yb^{3+} concentration of ~3.8×10^{21} per cubic centimeter, grown onto an un-doped $KY(WO_4)_2$ substrate. The pump absorption, luminescence decay, and small-signal gain are investigated under intense pumping conditions. Spectroscopic signatures of an energy-transfer process and of quenched ions, as well as thermal effects are observed. We present a gain model which takes into account excessive heat generated due to the abovementioned experimental observations. Based on finite-element calculations, we find that the net gain is significantly reduced due to, firstly, a fraction of Yb^{3+} ions not contributing to stimulated emission, secondly, a reduction of population inversion owing to a parasitic energy-transfer process and, thirdly, degradation of the effective transition cross-sections owing to device heating. Nevertheless, a signal enhancement of 8.1 dB was measured from the sample at 981 nm wavelength when pumping at 932 nm. The corresponding signal net gain of ~800 dB/cm, which was achieved without thermal management, is promising for waveguide amplifier operating without active cooling.

Keywords: Rare-earth-doped materials, integrated optics materials, optical amplifiers, ytterbium lasers.

1. INTRODUCTION

Potassium rare-earth double tungstate crystals doped with ytterbium, $KRE(WO_4)_2:Yb^{3+}$, have been widely used for microchip [1,2], mode-locked [3], and high-power lasers [4,5]. The $KRE(WO_4)_2:Yb^{3+}$ gain medium exhibits transition cross-sections significantly higher than those of many other Yb^{3+}-doped materials, such as $YAG:Yb^{3+}$ [6,7]. By use of a lattice-engineering approach [8,9,10], a crystalline waveguiding epitaxial layer with high amounts of Yb^{3+} ions can be grown onto an undoped $KY(WO_4)_2$ substrate, enabling efficient continuous-wave (CW) [11] and *Q*-switched [12,13,14] $KRE(WO_4)_2:Yb^{3+}$ planar waveguide lasers. By further micro-structuring of the $KRE(WO_4)_2:Yb^{3+}$ waveguide layer, low-threshold [15], high-efficiency [16], and tunable [17] channel waveguide lasers can be realized. A record-high net gain of 935 dB/cm at 981 nm wavelength was achieved in a $KRE(WO_4)_2$ waveguide amplifier with 47.5at.% Yb^{3+}, which is equivalent to a concentration as high as ~3.0×10^{21} cm^{-3} [18]. Such a compact waveguide amplifier operating at ~1000 nm wavelength is beneficial for scaling of short-reach interconnects in photonic integrated circuits, high-performance computing systems, and data centers [19,20,21,22]. As the net gain achieved in $KRE(WO_4)_2:Yb^{3+}$ is more than an order-of-magnitude higher than those of other singly-doped Nd^{3+} or Yb^{3+} gain media [23,24,25,26], it is worthwhile to investigate the gain properties of $KRE(WO_4)_2:Yb^{3+}$ epitaxial layers with further increased Yb^{3+} concentration.

Operating a heavily doped device under high excitation density is challenging. A power-dependent non-exponential decay behavior was reported in YbAG crystals, indicating the presence of a parasitic energy-transfer process [27]. Quenched ions with a short excited-state lifetime were identified in various Er^{3+}- [28,29,30,31] and Yb^{3+}-doped [32,33,34] materials. These ions can induce nonsaturable pump absorption [28,34]. Various abnormalities associated with thermal effects were

Solid State Lasers XXVIII: Technology and Devices, edited by W. Andrew Clarkson, Ramesh K. Shori, Proc. of SPIE Vol. 10896, 108961G · © 2019 SPIE · CCC code: 0277-786X/19/$18 · doi: 10.1117/12.2514806

reported in thin-disc gain media with high Yb^{3+} concentrations. An additional decay process with large heat generation was observed in a YAG:Yb^{3+} laser at high excitation density, resulting in limited gain and reduced laser efficiency [35]. Excessive heat generation leading to the termination of CW operation and a rapid decline in lasing power [36] was observed in a laser based on a $KLu(WO_4)_2$:(52at.%)Yb^{3+} epitaxial layer. A similar observation was reported from laser experiments in a $KYb(WO_4)_2$ crystal, in which a short pump-pulse duration was needed to minimize thermal effects [37]. Most of these abnormalities were studied based on device performance. There are limited reports on the investigation of their origin [38].

We investigate [39] the gain dynamics in a $KGd_{0.43}Yb_{0.57}(WO_4)_2$ (i.e., 57at.% Yb^{3+}) epitaxial layer, representing a high ytterbium concentration of ~3.8×10^{21} cm^{-3}. Power-dependent luminescence-decay and pump-absorption measurements are performed to identify potential energy-transfer and fast quenching processes. A gain model which accounts for an energy-transfer process, quenched ions, and thermal effects is established. The modeled and experimental gain results are compared to obtain further insight into the achievable gain in $KGd_{0.43}Yb_{0.57}(WO_4)_2$ without thermal management.

2. EXPERIMENTAL

A $KGd_{0.43}Yb_{0.57}(WO_4)_2$ layer was grown onto a $KY(WO_4)_2$ substrate by liquid-phase epitaxy [6,10], resulting in a layer thickness of ~ 32 µm after polishing. The sample was mounted on a small holder made of thin copper plates with a clear aperture of ~ 8.6 mm × 8.6 mm. No special thermal management was applied to the sample during all measurements. A confocal luminescence-lifetime measurement setup [40] was used for power-dependent luminescence-decay measurements. The confocal measurement suppresses radiation trapping [41] and allows for investigation of the decay-time behavior under high excitation density. A diode pump laser at 981 nm was modulated at 233 Hz with 50% duty cycle to allow for complete relaxation of the Yb^{3+} ions between two excitation pulses. The experimental setup for signal-enhancement measurement included a CW Ti:Sapphire laser at 932 nm for pumping at the local absorption peak of $KGd_{0.43}Yb_{0.57}(WO_4)_2$ at ~ 932 nm. The signal beam at ~ 981 nm, exploiting the high emission cross-section [6], with a bandwidth ≤ 1 nm from a supercontinuum light source passed through a monochromator was mechanically chopped at 233 Hz for lock-in detection to discriminate the detected 981 nm wavelength signal from spontaneous emission produced by the sample and from different background noise sources. A small launched signal power (< 100 nW) was used to ensure signal amplification within the small-signal-gain regime. Pump and signal beams were combined and focused perpendicularly onto the sample at $E \| N_m$ polarization using a microscope objective (MO). To ensure a good overlap of pump and signal beams, the foci were characterized using a beam profiler and the beam-expander optics were adjusted for optimal beam overlap. The residual optical beams passing through the sample were collected using another MO and directed to a spectrometer equipped with a cooled InGaAs detector. Combination of a pump filter with cutoff wavelength at 950 nm and the spectrometer ensured that only the 981 nm signal was detected. Pump-transmission measurements were performed with only the pump beam switched on, to deduce the pump power absorbed by the sample. Near-infrared luminescence spectra were measured using the same setup by launching only the pump beam. The luminescence spectra were corrected for spectral response of the detection system determined using a calibration lamp.

3. GAIN MODEL

Since the energy-level scheme of the Yb^{3+} ion consists only of the $^2F_{7/2}$ ground-state and the $^2F_{5/2}$ excited-state manifolds, a two-level system is used to model the gain and loss of optical beams. The Yb^{3+} ions excited to the upper Stark level of the $^2F_{5/2}$ manifold undergo a rapid relaxation to the lower Stark level of the same manifold. The gain model is modified from [28]. It takes into account two distinct classes of Yb^{3+} ions, namely active ions and quenched ions, which both participate in pump absorption. The active ions decay by infrared luminescence to the ground state with an excited-state luminescence lifetime τ_a. The quenched ions have a non-radiative lifetime τ_q which is significantly shorter than τ_a. The total density of active and quenched ions residing in the ground state and excited state follows

$$N_{0\,a/q} + N_{1\,a/q} = f_{a/q} N_{Yb} \tag{1}$$

where N_{Yb} is the density of Yb^{3+} ions and N_0 and N_1 are the respective density of ions in the ground state and excited state. The subscripts a and q indicate active and quenched ions, respectively. $f_{a/q}$ represents the fraction of active or quenched ions, with the boundary condition of $f_a + f_q = 1$. The rate constants of absorption and stimulated emission on the 932 nm pump transition, $R_{p,01}$ and $R_{p,10}$, and the 981 nm signal transition, $R_{s,01}$ and $R_{s,10}$, respectively, are calculated as [42,43]

$$R_{p,01} = I_p \sigma_{abs}(\lambda_p, T) \cdot \frac{\lambda_p}{hc}, \quad R_{p,10} = I_p \sigma_{em}(\lambda_p, T) \cdot \frac{\lambda_p}{hc}, \quad R_{s,01} = I_s \sigma_{abs}(\lambda_s, T) \cdot \frac{\lambda_s}{hc}, \quad R_{s,10} = I_s \sigma_{em}(\lambda_s, T) \cdot \frac{\lambda_s}{hc} \tag{2}$$

where I represents the intensity, h is Planck's constant, and c is the speed of light. σ_{abs} and σ_{em} are the effective absorption and emission cross-sections, respectively, at wavelength λ and temperature T. The subscripts p and s denote pump and signal, respectively. Considering that both pump and signal beams possess a Gaussian beam profile in the x-y plane, their lateral intensity profiles, $I_{p,s}$, can be modeled with

$$I_{p,s} = \left(2P_{p,s} \big/ \pi w_{p,s}{}^2\right) \exp\left[-2(x^2 + y^2) \big/ w_{p,s}{}^2\right] \tag{3}$$

where P represents the optical power and w denotes the Gaussian beam waist. The parameters N, σ, R, and I in Eqs. (1)–(3) are spatially dependent. The xyz discretization for these parameters is taken into account. The rate equations which govern the change of density of the Yb^{3+} ions in the two energy levels are

$$\frac{dN_{1\,a/q}}{dt} = \left(R_{p,01} + R_{s,01}\right) N_{0\,a/q} - \left(R_{p,10} + R_{s,10}\right) N_{1\,a/q} - \frac{N_{1\,a/q}}{\tau_{a/q}} - 2W_{ET}\left(N_{1\,a/q}\right)^2 \tag{4}$$

$$\frac{dN_{0\,a/q}}{dt} = -\frac{dN_{1\,a/q}}{dt} \tag{5}$$

Besides the pump and signal transitions which are typical for the rate equations of Yb^{3+}-doped materials, the model includes an energy-transfer (ET) process identified in our pump-dependent luminescence-decay measurements. The physical origin of this ET process is currently unknown. However, since the luminescence-decay curves exhibit the typical shape of a Bernoulli curve, see Eq. (7), we chose Grant's model [44] which assumes an infinitely fast energy-migration rate. The ET process is taken into account by the term $2W_{ET}N_1{}^2$, where W_{ET} is the macroscopic ET parameter. This is similar to a cooperative-upconversion process between two neighboring Yb^{3+} ions or an energy-transfer-upconversion process between neighboring Er^{3+} ions in the upper amplifier level [28]. Consequently, the evolution of excited-state population density after cut-off of pump power during luminescence-decay measurements is modeled with [45]

$$\frac{dN_{1\,a}(t)}{dt} = -\frac{N_{1\,a}(t)}{\tau_a} - 2W_{ET} N_{1\,a}{}^2(t) \tag{6}$$

which can be solved as

$$N_{1\,a}(t) = \frac{N_{1\,a}(0)\exp\left(-t/\tau_a\right)}{1 + 2W_{ET} N_{1\,a}(0)\tau_a\left[1 - \exp\left(-t/\tau_a\right)\right]} \tag{7}$$

$N_{1\,a}(0)$ represents the density of active excited ions at time zero. It can be estimated by varying the excitation conditions. The value of W_{ET} can be quantified via simultaneous fitting of luminescence-decay curves measured under different excitation conditions. The solutions of Eqs. (4)–(5) can be simplified in the case of small-signal amplification. The quenched ions only participate in the absorption of pump and signal photons. Under CW pumping, the steady-state condition $dN/dt = 0$ applies. Thus, $N_{1\,a}$ in Eq. (4) can be solved as

$$N_{1\,a} = \frac{-B_a + \sqrt{B_a{}^2 - 4AC_a}}{2A} \tag{8}$$

where

$$A = 2W_{ET}, \quad B_a = R_{p,10} + R_{p,01} + \frac{1}{\tau_a}, \quad C_a = -f_a N_{Yb} R_{p,01} \tag{9}$$

for calculations including the ET process, and

$$N_{1a} = \frac{R_{p,01}}{R_{p,01} + R_{p,10} + \tau_a^{-1}} \tag{10}$$

for calculations excluding the ET process. The evolution of pump power P_p and signal power P_s along the propagation direction z is calculated according to

$$\frac{dP_p}{dz} = \left[\sigma_{em,p} N_{1a} - \sigma_{abs,p}\left(N_{0a} + f_q N_{Yb}\right)\right] P_p - \alpha_p P_p \tag{11}$$

$$\frac{dP_s}{dz} = \left[\sigma_{em,s} N_{1a} - \sigma_{abs,s}\left(N_{0a} + f_q N_{Yb}\right)\right] P_s - \alpha_s P_s \tag{12}$$

where $\alpha_{p/s}$ is the propagation-loss coefficient in the medium and $\sigma_{abs/em,\,p/s}$ denotes $\sigma_{abs/em}(\lambda_{p/s}, T)$. Since the propagation loss for devices made of $KRE(WO_4)_2$:Yb^{3+} at ~1000 nm wavelength is typically < 0.04 dB/cm [15], both α_p and α_s are considered to be negligible (i.e., $\alpha_p = \alpha_s = 0$) as compared to the absorption and emission terms in Eqs. (11)–(12).

To account for thermal effects, the power per unit volume deposited as heat in the device is determined by [46,47]

$$Q_{th}(x,y,z) = \eta_h \alpha_{abs,p} I_p(0) \exp\left(-\alpha_{abs,p} z\right) \tag{13}$$

where η_h is the fractional heat load and $\alpha_{abs,\,p}$ is the pump-absorption coefficient with a magnitude given by the expression within the square bracket in Eq. (11). $I_p(0)$ represents the incident pump intensity at $z = 0$ with a Gaussian profile as described by Eq. (3). The fractional heat load η_h represents the fraction of absorbed pump power per unit volume which is converted into heat. It consists of the fractional heat loads originating in the quantum defect, η_{QD}, the ET process, η_{ET}, and the rapid quenching process, η_q:

$$\eta_h = f_a\left(\eta_{QD} + \eta_{ET}\right) + f_q \eta_q \tag{14}$$

The quantum defect is defined by the fractional amount of absorbed photon energy which is converted to heat due to the difference of energy between the absorbed and emitted photons

$$\eta_{QD} = 1 - \lambda_p / \lambda_m \tag{15}$$

where λ_m is the mean emission wavelength estimated using

$$\lambda_m(T) = \int \lambda \sigma_{em}(\lambda, T)\, d\lambda \Big/ \int \sigma_{em}(\lambda, T)\, d\lambda \tag{16}$$

λ_m is chosen, because, in contrast to a laser, an amplifier operating in the small-signal-gain regime does not possess a single dominating emission wavelength. The chosen values are $\eta_{QD} = \eta_{ET} = 6.4\%$ and $\eta_q = 100\%$ (for further explanations, see the Appendix). The temperature profile of the sample is governed by the heat-conduction equation and the boundary conditions between sample and external environment where heat exchange occur [48],

$$-k_{th} \nabla^2 T(x,y,z) = Q_{th}(x,y,z) \tag{17}$$

$$\frac{\partial T}{\partial n} = h_T\left(T_{ext} - T\right) \tag{18}$$

where k_{th} is the thermal conductivity, n is the normal to the boundary surface, h_T is the heat transfer coefficient, and T_{ext} is the external temperature of the thermal contact. The three-dimensional optical-beam and thermal profiles were solved using a finite-element method. Material parameters are given in [39].

4. RESULTS AND DISCUSSION

Luminescence-decay curves under different pump power P_p are shown in Fig. 1(a). At a low P_p of 1.44 mW, the decay curve is close to an exponential decay. With increasing P_p, the detected decay curves exhibit an increasingly non-exponential decay, indicating that an ET process is present. By simultaneously fitting the eight decay curves shown in Fig. 1(a) using Eq. (7), a W_{ET} value of 1.3×10^{-18} cm^3/s is extracted. The presence of an energy-transfer process in an Yb^{3+}-activated material is intriguing, as the Yb^{3+} ion has only two manifolds within the 4*f* sub-shell. A power-dependent non-exponential decay behavior similar to that observed in the present work was reported in YbAG crystals [27] and was attributed to cooperative energy transfer from two Yb^{3+} ions to an Yb^{2+} ion. However, the presence of Yb^{2+} has not been reported in $KRE(WO_4)_2$:Yb^{3+}, although it is known to exist in certain as-grown crystals such as YAG:Yb^{3+} [49] and LuAG:Yb^{3+} [50]. Since the experimental data can be well described by Bernoulli's Eq. (7), the energy transfer is possibly caused by cooperative upconversion involving two neighboring excited Yb^{3+} ions, jointly emitting one green photon [51]. However, we have detected only very weak green upconversion luminescence. At present, the exact physical mechanism responsible for the observed behavior remains unclear.

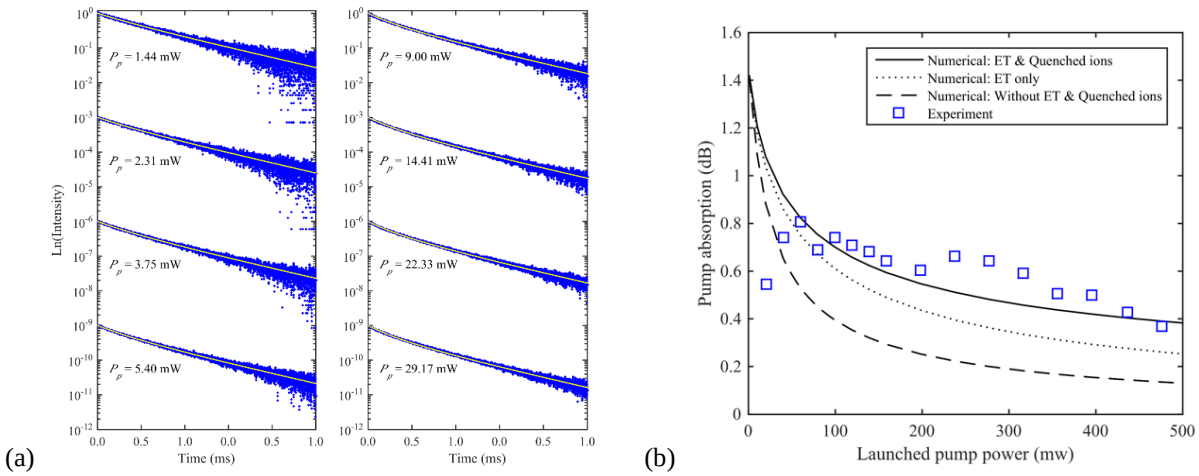

Figure 1. (a) Luminescence-decay curves (blue) measured with different launched diode-laser power P_p. The yellow lines represent fitted curves using Eq. (7). (b) Comparison of experimental pump-absorption data (squares) and pump-absorption results calculated with various settings (lines). The dashed line represents the modeled result without considering the ET process and quenched ions (i.e., $W_{ET} = 0$ and $f_q = 0$). The dotted line shows the modeled result which accounts for the ET process but not the quenched ions (i.e., $W_{ET} = 1.3 \times 10^{-18}$ cm^{3}s^{-1} and $f_q = 0$). The solid line is calculated with the consideration of both the ET process and quenched ions ($W_{ET} = 1.3 \times 10^{-18}$ cm^{3}s^{-1} and $f_q = 0.15$). (Figure taken from Ref. [39].)

It is apparent from Eq. (13) that heat generation in the sample depends on absorbed pump power. The pump absorption at 932 nm wavelength is investigated by comparing experimental and numerical results. The measured data points of pump absorption versus launched pump power are plotted in Fig. 1(b) as squares. The pump absorption is defined as

$$A_p = -10\log_{10}\left[P_p\left(t_{layer}\right)/P_p\left(0\right)\right] \tag{19}$$

where $P_p(0)$ is the launched Ti:Sapphire pump power at the front surface. $P_p(t_{layer})$ is the residual pump power at the rear surface. The calculated pump absorption using various sets of parameters are shown as lines in Fig. 1(b). These results take into account the pump-induced heating, the changes of effective transition cross-sections due to temperature-dependent Boltzmann populations and transition linewidths, as well as thermal conductivities due to the heat generated.

The result calculated without both ET process and quenched ions [dashed line in Fig. 1(b)] show a more intense saturation of pump absorption than the experimental results. The ET process, as identified in the previous sub-section, serves as an additional decay channel from the excited state. Therefore, the pump absorption (dotted line) is increased because a larger amount of ions is available in the ground state. Additional nonsaturable pump absorption is addressed by considering that ~15% of the Yb^{3+} ions are rapidly quenched, in addition to the ET process. In Al_2O_3:Yb^{3+}, a similar nonsaturable absorption was observed and attributed to 11% of Yb^{3+} ions being quenched at a dopant concentration of 6.6×10^{20} cm^{-3} [34]. The pump absorption calculated under consideration of these two factors is shown as a solid line in Fig. 1(b) and is in reasonable agreement with the experimental results.

Figure 2(a) shows the near-infrared luminescence spectra at various launched pump-power values P_p. Three emission peaks are observed at ~ 981 nm, ~ 1000 nm, and ~ 1023 nm wavelengths, which correspond to the $E_{10} \rightarrow E_{00}$, $E_{10} \rightarrow E_{01}$, and $E_{10} \rightarrow E_{02}$ transitions, respectively, see the inset of Fig. 2(a). With increasing pump power, a smoothening emission spectrum is observed and the emission peaks at 1000 nm and 1023 nm wavelengths become less distinguishable. In addition, the ratio of the magnitude of the 981 nm emission peak to that of the 1000 nm emission peak decreases with increasing P_p. Analysis of the spectra was performed via multiple-peak fitting by assuming three Lorentzian peaks. The full-width-at-half-maximum (FWHM) values for the emission peak at 981 nm for different P_p values are plotted in Fig. 2(b). A significant increase in FWHM is evident. The linewidth broadening is in line with the temperature-dependent behavior of the emission cross-section spectra [6], signifying that a thermal effect is present in the gain medium even under low P_p.

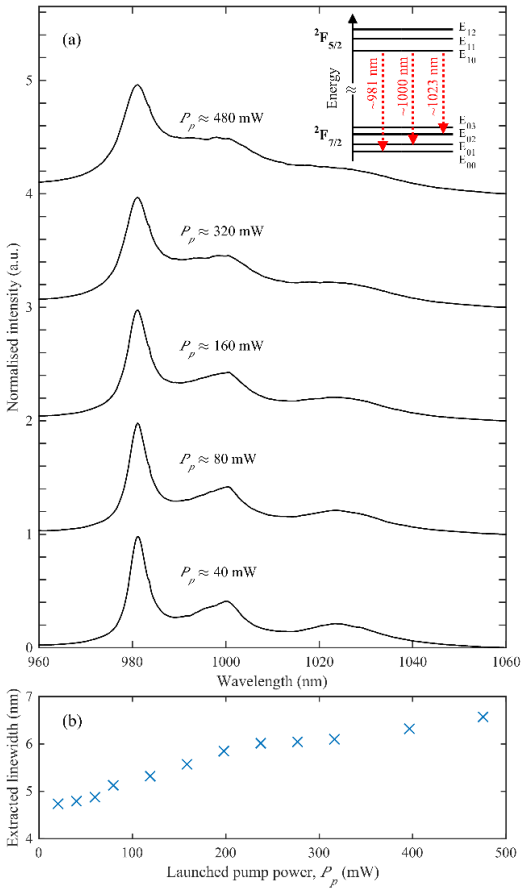

Figure 2. (a) Normalized luminescence spectra recorded with different Ti:Sapphire launched pump power P_p. The inset illustrates the relevant transitions contributing to a large part of the observed emission at the corresponding wavelength. (b) Evolution of the linewidth (FWHM) of the decomposed peak at ~ 981 nm with increasing P_p. (Figure taken from Ref. [39].)

The experimental and modeled signal-enhancement results are shown in Fig. 3(a). The maximum signal enhancement measured at ~475 mW launched pump power is 8.13 dB. The modeled signal enhancement under consideration of the ET process, 15% quenched ions, and thermal effects is in reasonable agreement with the experimental results. The calculation shows that T_p can rise from 27˚C with pump off to 62.8˚C at P_l = 475 mW. Considering in Eq. (22) the reduced absorption cross-section of 1.058×10^{-19} cm^2 calculated at T_p = 62.8˚C, a total signal absorption of 5.59 dB is deduced. Consequently, a peak net-gain value of 2.54 dB, or 793.75 dB/cm, is obtained based on the signal-enhancement data.

Comparison of the modeled gain in Fig. 3(b) reveals a marked difference in gain performance when considering the usual gain model for Yb^{3+}-doped media and our proposed model. The usual gain model does not include an ET process and quenched ions, hence the heat generation is mainly owing to the quantum defect which is inherently low in Yb^{3+}-doped devices. The peak gain deduced from such a model (dashed line) is ~ 1900 dB/cm at P_l = 500 mW. Our gain model includes

an ET process, which causes depletion of the excited-state population. Consideration of 15% of quenched ions implies that only the remaining 85% of active ions are participating in the signal-amplification process. The increased heating reduces the transition cross-sections. The gain calculated with the proposed model (solid line) is effectively clamped to ~ 820 dB/cm at 500 mW of launched pump power. Nevertheless, the net gain per unit length is more than an order of magnitude higher than in other Yb^{3+}- or Nd^{3+}-doped waveguide amplifiers [23,24,25,26] and comparable to the modal gain of III-V semiconductor amplifiers.

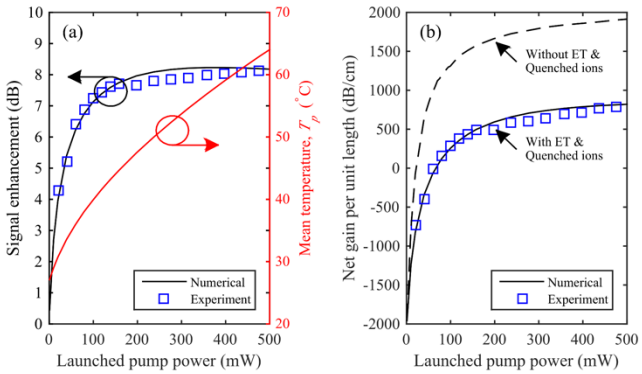

Figure 3. (a) Experimental and modeled signal enhancement. The calculated mean temperature within the pump volume is shown on the right y-axis. (b) Corresponding results of net gain per unit length. The net gain per unit length calculated without considering the ET process and quenched ions is shown in (b) as a dashed line. (Figure taken from Ref. [39].)

5. SUMMARY

The optical properties of a $KGd_{0.43}Yb_{0.57}(WO_4)_2$ epitaxial film with an Yb^{3+} concentration as high as ~ 3.8×10^{21} cm^{-3} were examined. A parasitic energy-transfer process and quenched ions were observed under intense excitation conditions, and the relevant parameters were quantified. The broadening of emission spectra signifies the presence of thermal effects even at low pump power. A gain model which takes into account the energy-transfer process, quenched ions, and thermal effects provides insight into the impact of these non-desired effects on the attainable gain in an epitaxial film with high Yb^{3+} concentration. The temperature of the pumped volume may elevate to >60˚C. A peak signal enhancement of 8.13 dB is obtained at 981 nm. A peak net-gain of ~800 dB/cm is attainable.

REFERENCES

[1] Kuleshov, N. V., Lagatsky, A. A., Podlipensky, A. V., Mikhailov, V. P., and Huber, G. "Pulsed laser operation of Yb-doped $KY(WO_4)_2$ and $KGd(WO_4)_2$," Opt. Lett. **22**(17), 1317-1319 (1997).

[2] Hellström, J. E., Jacobsson, B., Pasiskevicius, V., and Laurell, F. "Quasi-two-level Yb:KYW laser with a volume Bragg grating," Opt. Express **15**(21), 13930-13935 (2007).

[3] Chang, M. T., Liang, H. C., Su, K. W., and Chen, Y. F. "Dual-comb self-mode-locked monolithic Yb:KGW laser with orthogonal polarizations," Opt. Express **23**(8), 10111-10116 (2015).

[4] Liu, J., Petrov, V., Mateos, X., Zhang, H., and Wang, J. "Efficient high-power laser operation of Yb:$KLu(WO_4)_2$ crystals cut along the principal optical axes," Opt. Lett. **32**(14), 2016-2018 (2007).

[5] Petermann, K., Fagundes-Peters, D., Johannsen, J., Mond, M., Peters, V., Romero, J. J., Kutovoi, S., Speiser, J., and Giesen, A. "Highly Yb-doped oxides for thin-disc lasers," J. Cryst. Growth **275**(1-2), 135-140 (2005).

[6] Yong, Y. S., Aravazhi, S., Vázquez-Córdova, S. A., Carjaval, J. J., Díaz, F., Herek, J. L., García-Blanco, S. M., and Pollnau, M. "Temperature-dependent absorption and emission of potassium double tungstates with high ytterbium content," Opt. Express **24**(23), 26825-26837 (2016).

[7] Koerner, J., Vorholt, C., Liebetrau, H., Kahle, M., Kloepfel, D., Seifert, R., Hein, J., and Kaluza, M. C. "Measurement of temperature-dependent absorption and emission spectra of Yb:YAG, Yb:LuAG, and Yb:CaF_2 between 20°C and 200°C and predictions on their influence on laser performance," J. Opt. Soc. Am. B **29**(9), 2493-2502 (2012).

[8] Gardillou, F., Romanyuk, Y. E., Borca, C. N., Salathé, R. P., and Pollnau, M. "Lu, Gd codoped $KY(WO_4)_2$:Yb epitaxial layers: towards integrated optics based on $KY(WO_4)_2$," Opt. Lett. **32**(5), 488-490 (2007).
[9] Pollnau, M., Romanyuk, Y. E., Gardillou, F., Borca, C. N., Griebner, U., Rivier, S., and Petrov, V. "Double tungstate lasers: From bulk toward on-chip integrated waveguide devices," IEEE J. Sel. Top. Quantum Electron. **13**(3), 661-671 (2007).
[10] Aravazhi, S., Geskus, D., van Dalfsen, K., Vázquez-Córdova, S. A., Grivas, C., Griebner, U., García-Blanco, S. M., and Pollnau, M. "Engineering lattice matching, doping level, and optical properties of $KY(WO_4)_2$:Gd, Lu, Yb layers for a cladding-side-pumped channel waveguide laser," Appl. Phys. B **111**(3), 433-446 (2013).
[11] Geskus, D., Aravazhi, S., Bernhardi, E., Grivas, C., Harkema, S., Hametner, K., Günther, D., Wörhoff, K., and Pollnau, M. "Low-threshold, highly efficient Gd^{3+}, Lu^{3+} co-doped $KY(WO_4)_2$:Yb^{3+} planar waveguide lasers," Laser Phys. Lett. **6**(11), 800-805 (2009).
[12] Kim, J. W., Choi, S. Y., Yeom, D. I., Aravazhi, S., Pollnau, M., Griebner, U., Petrov, V., and Rotermund, F. "Yb:KYW planar waveguide laser Q-switched by evanescent-field interaction with carbon nanotubes," Opt. Lett. **38**(23), 5090-5093 (2013).
[13] Kim, J. W., Choi, S. Y., Aravazhi, S., Pollnau, M., Griebner, U., Petrov, V., Bae, S., Ahn, K. J., Yeom, D. I., and Rotermund, F. "Graphene Q-switched Yb:KYW planar waveguide laser," AIP Adv. **5**(1), 017110 (2015).
[14] Bain, F. M., Lagatsky, A. A., Kurilchick, S. V., Kisel, V. E., Guretsky, S. A., Luginets, A. M., Kalanda, N. A., Kolesova, I. M., Kuleshov, N. V., Sibbett, W., and Brown, C. T. A. "Continuous-wave and Q-switched operation of a compact, diode-pumped Yb^{3+}:$KY(WO_4)_2$ planar waveguide laser," Opt. Express **17**(3), 1666-1670 (2009).
[15] Geskus, D., Aravazhi, S., Grivas, C., Wörhoff, K., and Pollnau, M. "Microstructured $KY(WO_4)_2$:Gd^{3+}, Lu^{3+}, Yb^{3+} channel waveguide laser," Opt. Express **18**(9), 8853-8858 (2010).
[16] Geskus, D., Bernhardi, E. H., van Dalfsen, K., Aravazhi, S., and Pollnau, M. "Highly efficient Yb^{3+}-doped channel waveguide laser at 981 nm," Opt. Express **21**(11), 13773-13778 (2013).
[17] Geskus, D., Aravazhi, S., Wörhoff, K., and Pollnau, M. "High-power, broadly tunable, and low-quantum-defect $KGd_{1-x}Lu_x(WO_4)_2$:Yb^{3+} channel waveguide lasers," Opt. Express **18**(25), 26107-26112 (2010).
[18] Geskus, D., Aravazhi, S., García-Blanco, S. M., and Pollnau, M. "Giant optical gain in a rare-earth-ion-doped microstructure," Adv. Mater. **24**(10), OP19-OP22 (2012).
[19] Doany, F. E., Schow, C. L., Baks, C. W., Kuchta, D. M., Pepeljugoski, P., Schares, L., Budd, R., Libsch, F., Dangel, R., Horst, F., Offrein, B. J., and Kash, J. A. "160 Gb/s bidirectional polymer-waveguide board-level optical interconnects using CMOS-based transceivers," IEEE Trans. Adv. Packag. **32**(2), 345-359 (2009).
[20] Héroux, J. B., Kise, T., Funabashi, M., Aoki, T., Schow, C. L., Rylyakov, A. V., and Nakagawa, S. "Energy-efficient 1060-nm optical link operating up to 28 Gb/s," J. Lightwave Technol. **33**(4), 733-740 (2015).
[21] Nasu, H., Ishikawa, Y., Nekado, Y., Yoshihara, M., Izawa, A., Uemura, T., and Takahashi, K. "1060-nm VCSEL-based parallel-optical modules for short link applications," in *Optical Fiber Communication (OFC), collocated National Fiber Optic Engineers Conference, 2010 Conference on (OFC/NFOEC)*, (IEEE, 2010), OThC1.
[22] Yang, J., Lamprecht, T., Wörhoff, K., Driessen, A., Horst, F., Offrein, B. J., Ay, F., and Pollnau, M. "Integrated optical backplane amplifier," IEEE J. Sel. Top. Quantum Electron. **17**(3), 609-616 (2011).
[23] Aghajani, A., Murugan, G. S., Sessions, N. P., Pearce, S. J., Apostolopoulos, V., and Wilkinson, J. S. "Spectroscopy of ytterbium-doped tantalum pentoxide rib waveguides on silicon," Opt. Mater. Express **4**(8), 1505-1514 (2014).
[24] Yang, J., van Dalfsen, K., Wörhoff, K., Ay, F., and Pollnau, M. "High-gain Al_2O_3:Nd^{3+} channel waveguide amplifiers at 880 nm, 1060 nm, and 1330 nm," Appl. Phys. B **101**(1), 119-127 (2010).
[25] Yang, J., Diemeer, M. B. J., Sengo, G., Pollnau, M., and Driessen, A. "Nd-doped polymer waveguide amplifiers," IEEE J. Quantum Electron. **46**(7), 1043-1050 (2010).
[26] Tan, Y., Luan, Q., Liu, F., Akhmadaliev, S., Zhou, S., and Chen, F. "Swift carbon ion irradiated Nd:YAG ceramic optical waveguide amplifier," Opt. Express **21**(12), 13992-13997 (2013).
[27] Fagundes-Peters, D., Martynyuk, N., Lünstedt, K., Peters, V., Petermann, K., Huber, G., Basun, S., Laguta, V., and Hofstaetter, A. "High quantum efficiency YbAG-crystals," J. Lumin. **125**(1–2), 238-247 (2007).
[28] Agazzi, L., Wörhoff, K., and Pollnau, M. "Energy-transfer-upconversion models, their applicability and breakdown in the presence of spectroscopically distinct ion classes: A case study in amorphous Al_2O_3:Er^{3+}," J. Phys. Chem. C **117**, 6759-6776 (2013).
[29] Banerjee, S., Baker, C. C., Steckl, A. J., and Klotzkin, D. "Optical properties of Er in Er-doped $Zn_2Si_{0.5}Ge_{0.5}O_4$ waveguide amplifiers," J. Lightwave Technol. **23**(3), 1342-1349 (2005).

[30] Delevaque, E., Georges, T., Monerie, M., Lamouler, P., and Bayon, J. F. "Modeling of pair-induced quenching in erbium-doped silicate fibers," IEEE Photon. Technol. Lett. **5**(1), 73-75 (1993).
[31] Maurice, E., Monnom, G., Dussardier, B., and Ostrowsky, D. B. "Clustering-induced nonsaturable absorption phenomenon in heavily erbium-doped silica fibers," Opt. Lett. **20**(24), 2487-2489 (1995).
[32] Paschotta, R., Nilsson, J., Barber, P. R., Caplen, J. E., Tropper, A. C., and Hanna, D. C. "Lifetime quenching in Yb-doped fibres," Opt. Commun. **136**(5-6), 375-378 (1997).
[33] Burshtein, Z., Kalisky, Y., Levy, S. Z., Le Boulanger, P., and Rotman, S. "Impurity local phonon nonradiative quenching of Yb^{3+} fluorescence in ytterbium-doped silicate glasses," IEEE J. Quantum Electron. **36**(8), 1000-1007 (2000).
[34] Agazzi, L., Bernhardi, E. H., Wörhoff, K., and Pollnau, M. "Impact of luminescence quenching on relaxation-oscillation frequency in solid-state lasers," Appl. Phys. Lett. **100**(1), 011109 (2012).
[35] Larionov, M., Schuhmann, K., Speiser, J., Stolzenburg, C., and Giesen, A. "Nonlinear decay of the excited state in Yb:YAG," in *Advanced Solid-State Photonics 2005*, Technical Digest (Optical Society of America, 2005), TuB49.
[36] Petrov, V., Pujol, M. C., Mateos, X., Silvestre, Ò., Rivier, S., Aguiló, M., Solé, R. M., Liu, J., Griebner, U., and Díaz, F. "Growth and properties of $KLu(WO_4)_2$, and novel ytterbium and thulium lasers based on this monoclinic crystalline host," Laser Photonics Rev. **1**(2), 179-212 (2007).
[37] Klopp, P., Griebner, U., Petrov, V., Mateos, X., Bursukova, M. A., Pujol, M. C., Sole, R., Gavalda, J., Aguilo, M., Güell, F., Massons, J., Kirilov, T., and Diaz, F. "Laser operation of the new stoichiometric crystal $KYb(WO_4)_2$," Appl. Phys. B **74**(2), 185-189 (2002).
[38] Brandt, C., Fredrich-Thornton, S. T., Petermann, K., and Huber, G. "Photoconductivity in Yb-doped oxides at high excitation densities," Appl. Phys. B **102**(4), 765-768 (2011).
[39] Yong, Y. S., Aravazhi, S., Vázquez-Córdova, S. A., Herek, J. L., García-Blanco, S. M., and Pollnau, M. "Gain dynamics in a highly ytterbium-doped potassium double tungstate epitaxial layer," J. Opt. Soc. Am. B **35**(9), 2176-2185 (2018).
[40] Yong, Y. S., Aravazhi, S., Vázquez-Córdova, S. A., Carvajal, J. J., Díaz, F., Herek, J. L., García-Blanco, S. M., and Pollnau, M. "Direct confocal lifetime measurements on rare-earth-doped media exhibiting radiation trapping," Opt. Mater. Express **7**(2), 527 (2017).
[41] Sumida, D. S., and Fan, T. Y. "Effect of radiation trapping on fluorescence lifetime and emission cross section measurements in solid-state laser media," Opt. Lett. **19**(17), 1343-1345 (1994).
[42] Paschotta, R., Nilsson, J., Tropper, A. C., and Hanna, D. C. "Ytterbium-doped fiber amplifiers," IEEE J. Quantum Electron. **33**(7), 1049-1056 (1997).
[43] Jacobsson, B. "Experimental and theoretical investigation of a volume-Bragg-grating-locked Yb:KYW laser at selected wavelengths," Opt. Express **16**(9), 6443-6454 (2008).
[44] Grant, W. J. C. "Role of rate equations in the theory of luminescent energy transfer," Phys. Rev. B **4**(2), 648-663 (1971).
[45] Golding, P. S., Jackson, S. D., King, T. A., and Pollnau, M. "Energy transfer processes in Er^{3+}-doped and Er^{3+},Pr^{3+}-codoped ZBLAN glasses," Phys. Rev. B **62**(2), 856-864 (2000).
[46] Innocenzi, M. E., Yura, H. T., Fincher, C. L., and Fields, R. A. "Thermal modeling of continuous- wave end-pumped solid- state lasers," Appl. Phys. Lett. **56**(19), 1831-1833 (1990).
[47] Loiko, P. A., Yumashev, K. V., Kuleshov, N. V., and Pavlyuk, A. A. "Comparative thermal analysis of Nd- and Yb-doped YAG and KGdW laser crystals under diode- and flashlamp-pumping," Opt. Laser Technol. **44**(7), 2232-2237 (2012).
[48] Chénais, S., Druon, F., Forget, S., Balembois, F., and Georges, P. "On thermal effects in solid-state lasers: The case of ytterbium-doped materials," Prog. Quant. Electron. **30**(4), 89-153 (2006).
[49] Xu, X., Zhao, Z., Song, P., Zhou, G., Xu, J., and Deng, P. "Structural, thermal, and luminescent properties of Yb-doped $Y_3Al_5O_{12}$ crystals," J. Opt. Soc. Am. B **21**(3), 543-547 (2004).
[50] Luo, D., Zhang, J., Xu, C., Yang, H., Lin, H., Zhu, H., and Tang, D. "Yb:LuAG laser ceramics: a promising high power laser gain medium," Opt. Mater. Express **2**(10), 1425-1431 (2012).
[51] Nakazawa, E., and Shionoya, S. "Cooperative luminescence in $YbPO_4$," Phys. Rev. Lett. **25**(25), 1710-1712 (1970).